Numerical Modeling of the Gob Loading Mechanism in Longwall Coal Mines

Khaled Morsy, Graduate Research Assistant
Syd Peng, Chairman and C.T. Holland Professor
West Virginia University
Department of Mining Engineering
Morgantown, WV

Abstract

Longwall mining is one of the most widely practiced underground coal mining method. The behavior of the longwall gob is very critical in the understanding of the complex ground response to longwall mining. In the limited data available, the values of gob moduli used in numerical modeling ranged from 1,000 psi to over 300,000 psi. Such a wide variation in moduli would greatly affect the results of the numerical analysis. A better understanding of the behavior of the gob will allow numerical models to be more accurate for simulating longwall mining conditions.

In this study, a gob model based on the Terzaghi's model was incorporated into the comprehensive finite element package, ABAQUS, to simulate the loading behavior of longwall gob material. A case study was used to verify the proposed gob model.

Background

As the longwall face moves forward, shields are advanced and the roof is allowed to cave behind the face. As the roof falls, the volume of caved materials or gob expands upward until it comes in contact with the sagging roof strata. As a result, the following five distinct stress zones may be defined (Figure 1).

Zone I - Undisturbed area of coal seam;
Zone II - Region of front and side abutment pressures;
Zone III- The exposed area between the face and gob;
Zone IV- The transition region in the gob area in which the broken strata is being compressed, and the degree of compaction increases with increasing distance from the face line;
Zone V - The region where the gob is fully compacted and the gob pressure equals to the primary (virgin) stress.

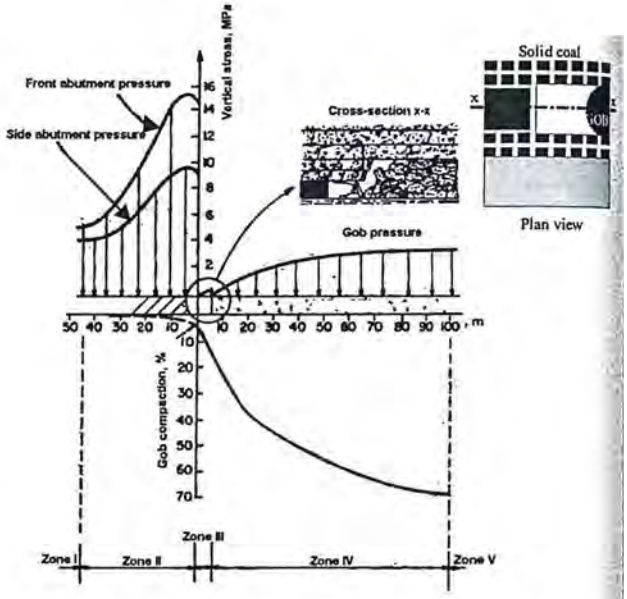

Figure 1 Probable distribution of strata pressure in the vicinity of the longwall face, (modified from Unrug et al., 1982)

Peng et al., (1980) performed three-dimensional finite element analysis to study the supporting role of the gob materials. The materials used in these models were assumed to be isotropic, homogeneous, and elastic. They divided the gob into three major zones:

1. Well-packed zone which is the center portion of the gob;
2. Packed zone which is on both sides of the well packed zone;
3. Loosely packed zone which is between the packed zone and ribsides.

They found that the front and side abutment pressures are reduced considerably due to the support offered by the gob. However they also found that the reduction of abutment pressure is

not sensitive to the degree of packing of the gob material, the height of caving, and the height of the fractured zone as long as the gob materials offers support to the overlying strata. Based on these findings, they used a "rule of thumb" for estimating the gob modulus which was estimated to range from 1/100 to 1/57 of the intact roof rock modulus depending upon how well the gob was packed.

Gob Pressure

At the start of coalface retreat operation, when the roof rocks start to cave in the gob, only the weight of the caved material will form the gob pressure. Also, a pressure arch will develop across the solid coal on both sides of the panel and a de-stressed zone above the gob area will be developed. As the longwall face retreats and the caving process continues, the caved materials pile up and the dimensions of the pressure arch increase. When the width of the pressure arch reaches the "maximum width" over which the main roof load can no longer be transferred to the solid coal perimeters, the main roof breaks. After this first break, the thickness of the loose caved rocks on the floor increases with the increase in the mined-out span. Ultimately, due to the combined effect of bulking, roof sag, and floor heave, the caved material comes into contact with the roof-and takes load from the upper strata. As the mining progresses further, the roof is lowered more firmly on the caved material. This roof settlement causes the gradual compaction of the gob material. Experience shows that once the extracted span is fairly large, the caving, re-compaction and roof sagging often progresses in repeatable cycles while the longwall face retreats.

Whittaker (1974) found that the gob pressure builds up until the cover load is reached at a distance of 0.3-0.4 time the seam depth from the solid abutments. Wilson (1982) assumed that the gob pressure is redistributed linearly across the active gob with zero stress at its edge and increasing to the original cover pressure at a distance of 0.2-0.3 times the overburden depth.

Whittaker and Singh (1979) indicated that the gob pressure starts to build up at a distance of 120 ft behind the face, and that it does not reach the cover load even after the face has advanced for a distance equal to the mining depth. Whether the gob pressure reaches the overburden pressure or not depends mainly on the panel width. If the panel is too narrow, the upper unbroken strata will be bridged between side abutments on both sides of the panel resulting in gob pressure being more or less the weight of rock up to the caving height.

Trueman (1990) performed two-dimensional finite element analysis to study the behavior of longwall coal mining gob material. He concluded that at a given geologic condition, the cover load would be reached in the gob at a fixed distance irrespective of mining depth. Also, he found that this distance mainly depends on the caving height.

Field measurements of gob loading have been conducted under varying sets of geological conditions. Campoli et al., (1993) investigated the longwall gob behavior in the 2,200 ft deep Pocahontas No. 3 coal seam. The floor pressure measurements showed a return to full overburden pressure at approximately 0.2 time the overburden depth. In a South African potash mine, Oyanguren (1972) concluded that at a distance of about 0.9 time the depth of overburden behind the face, the ground above the longwall gob was stabilized and the pressure on the gob floor had reached the overburden pressure.

Terzaghi's Model of Gob Material

Although the material making up the gob is the same as the immediate roof strata, the environment is different and the gob material can be considered as a different material from the in-situ rock and acts differently. Several authors have attempted to quantify the properties of gob material (Pappas and Mark, 1993).

Generally speaking, the gob material is strain hardening, i.e. the modulus of deformation increases with increasing compaction. There are two models available that can describe the hardening behavior of the gob material, namely; Salamon's model (Salamon, 1990) and Terzaghi's model (Pappas and Mark, 1993).

Terzaghi's approach assumes that the tangent Young's modulus of the granular material is a linear function of the applied normal stress.

$$E_t = E_o + a\sigma \tag{1}$$

where E_t = tangent Young's modulus;
σ = normal stress;
a = constant;
E_o = initial Young's modulus.

E_o is estimated as a ratio of the intact modulus E_i

$$E_o = R_o E_i \tag{2}$$

where, R_o is a constant.

The differential equation between normal stress σ and normal strain ε is

$$d\sigma = E_t d\varepsilon \tag{3}$$

Combining equations 1and 3 yields

$$d\varepsilon = \frac{d\sigma}{R_o E_i + a\sigma} \tag{4}$$

Integrating Equation 4 yields

$$\varepsilon = \frac{1}{a}\ln\left(R_o E_i + a\sigma\right) + c \tag{5}$$

where c is the constant of the integration and can be determined using the following initial condition:

$$\text{at } \varepsilon = 0;\ \sigma = 0 \tag{6}$$

Hence;

$$c = -\frac{\ln\left(R_o E_i\right)}{a} \tag{7}$$

$$\varepsilon = \frac{1}{a}\ln\left(1 + \frac{a}{R_o E_i}\sigma\right) \tag{8}$$

Rearranging Equation 8, the following stress-strain relation for the gob material is obtained:

$$\sigma = \frac{R_o E_i}{a}\left(e^{\varepsilon a} - 1\right) \qquad (9)$$

Pappas and Mark, (1993) evaluated the behavior of gob material experimentally. By comparing Terzaghi's model with laboratory data, they concluded that this model could describe the compressive behavior of gob material.

Implementation of Terzaghi's Model in FE Models

To define the Terzaghi's model, Equation 9, the constant "a" should be determined. Solving Equation 9 in terms of the secant modulus E_s:

$$E_s = \frac{\sigma}{\varepsilon} = \frac{a\sigma}{\ln\left(1 + \frac{a}{R_o E_i}\sigma\right)} \qquad (10)$$

It is assumed that the virgin stress σ_v could be recovered in the compacted region of the gob. Therefore the secant modulus of compacted gob $E_{s,v}$ subjected to the virgin stress σ_v, can be expressed as follows:

$$E_{s,v} = \frac{a\sigma_v}{\ln\left(1 + \frac{a}{R_o E_i}\sigma_v\right)} \qquad (11)$$

The secant modulus $E_{s,v}$ will be estimated as follows

$$E_{s,v} = \frac{nH\sigma_v}{\delta} \qquad (12)$$

where, n is the gob height factor which is the ratio between the gob height to the mined seam thickness, H.

δ is the maximum gob compaction in unit length.

Combining Equations 11 and 12, the constant "a" can be determined iteratively from the following expression:

$$a = \frac{nH}{\delta} \times \ln\left(1 + \frac{a}{R_o E_i}\sigma_v\right) \qquad (13)$$

In order to define the Terzaghi's model for gob elements in the finite element models, the stress-strain curve is divided into "n" points (Figure 2). At any point $k(\varepsilon_k, \sigma_k)$, the secant modulus $E_{s,k}$ is evaluated using Equation 10 and the corresponding strain energy density W_k is determined by:

$$W_k = \frac{1}{2}\varepsilon_k \sigma_k \qquad (14)$$

The parametric relationship between the strain energy and secant modulus for gob elements (Figure 3) can be defined for the gob elements.

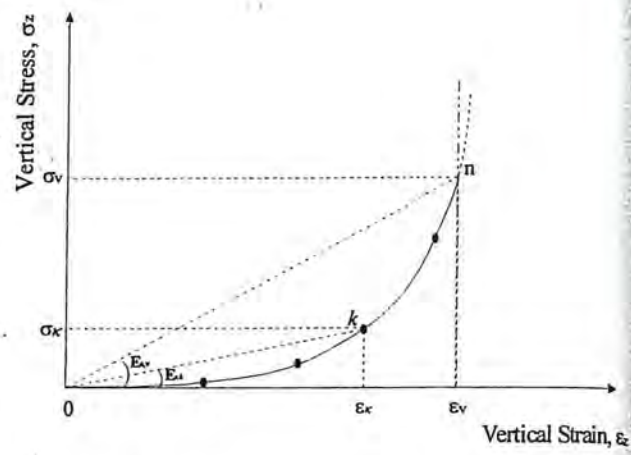

Figure 2 Stress-strain relationship for Terzagh's model.

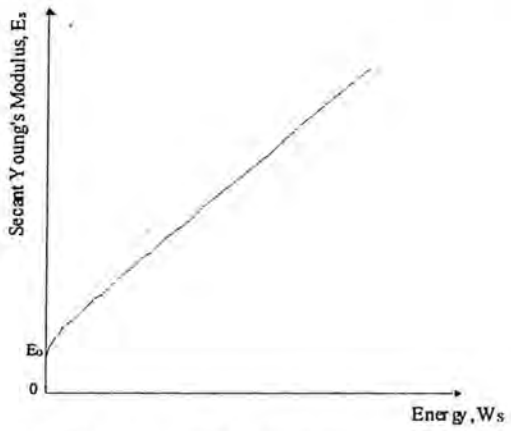

Figure 3 Strain energy density vs. secant Young's modulus for Terzaghi's model.

During the model solution, the parametric relationship (Figure 3) will be used to update the modulus of elasticity of gob elements according to their strain energies. Depending on the applied state of stress, the strain energy density of the gob elements are estimated using the following equation:

$$W = \frac{1}{2E_s}\left[\sigma_1^2 + \sigma_2^2 + \sigma_3^2 - 2\nu\left(\sigma_1\sigma_2 + \sigma_2\sigma_3 + \sigma_1\sigma_3\right)\right] \qquad (15)$$

where σ_1, σ_2 and σ_3 are maximum, intermediate and minimum principal stresses, respectively

Case Study

The mine for the verification of the gob model is located in Buchanan County, Virginia (Figure 4a). Several panels in this mine had been extensively instrumented for bump analysis (Campoli et al., 1993). The study area is located at the gateroad system between the 9th and 10th panels South (Figure 4a).

The mine extracts the Pocahontas No. 3 Coalbed, which averages 5.5 ft in thickness (Figure 4b). In the study area, the average overburden depth is 2,200 ft. The immediate roof consists of a widely jointed siltstone overlain by very stiff massive sandstone. The siltstone is 60 ft and the sandstone ranges from 210 ft to 230 ft thick. The mine floor consists of a combination of very competent siltstone and sandstone. The horizontal principal stresses are approximately 3,400 psi and 1,500 psi in the north-south and east-west directions, respectively.

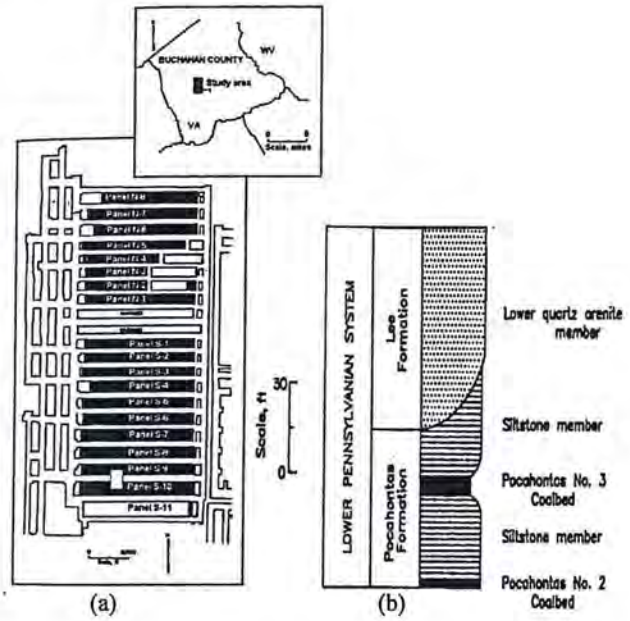

Figure 4 a. Mine location and panel layout, b. Stratigraphic column, Campoli et al., (1993).

The longwall panels associated with this study were 600 ft wide by 6,000 ft long, and developed using 4-entry yield-abutment-yield pillar system. The gateroad system was 238 ft wide consisting of a 20 ft x 80 ft yield pillar on either side of a 120 ft x 180 ft abutment pillar.

As part of a detailed instrumentation study in this mine (Campoli et al., 1993), a total of eighteen 3-in diameter BPF's were installed in the floor below panels S-9 and S-10. All these instruments were on a line approximately 3,800 ft from the setup rooms of panels S-9 and S-10 (Figure 5). The longwall gob floor loading was monitored throughout the whole panel S-9 when it was being mined and stopped after panel S-10 had passed the measuring station by 60 ft.

Finite Element Model

The ABAQUS finite element code was employed to simulate the longwall retreating steps. Three-dimensional finite element models with 8-node brick elements and six-node tetrahedron elements were used throughout all the analysis. The FE model consisted of half of panel S-9 and S-10 and the gateroad system.

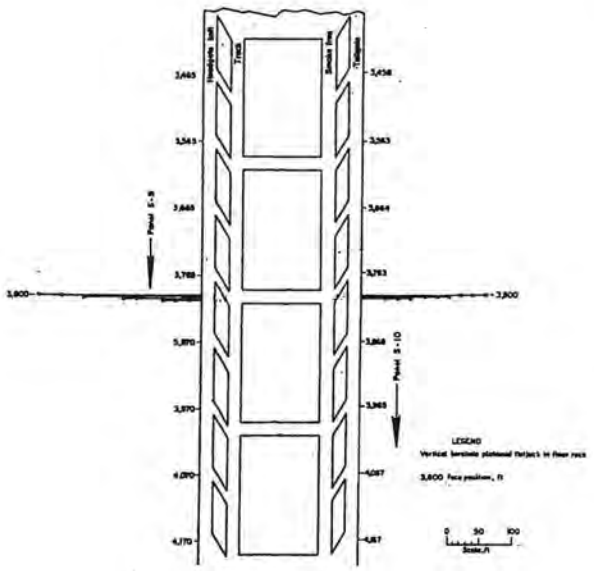

Figure 5 Underground study area, Campoli et al., (1993).

The dimension of the model was 840 ft x 930 ft x 550.5 ft (Figure 6). All the four side boundaries and the bottom boundary of the model were roller-constrained. A large number of elements and nodes (48,692 and 50,048, respectively) were used in the model. Linear elastic material properties have been assigned for the model except for the gob material. The gob height was predefined to be 6 times the seam thickness.

The gob model parameters (n, a, R_o and δ) are selected to ensure that the virgin stress σ_v is approximately recovered at a distance of 0.2-0.3 of the overburden depth from the panel ribs. A try and error approach was used to define the gob parameters (n=6, $a = 354.57$, R_o=0.001 and $\delta = 0.4884$ ft).

The model was solved in thirteen steps. In the first step, the gob elements were deactivated and the geostatic stress condition was applied. The gateroads were developed in the second step. Steps No. 3 to 8 and Steps No. 9 to 13 were assigned to simulate the activation of gob material and longwall retreat of panel S-9 and panel S-10, respectively. The retreat plan is shown in Figure 7.

Analysis and Discussions

The analysis of the FE model results was conducted in three stages. In the first stage, a detailed analysis was conducted for the gob behavior at retreat step No.5 of panel S-9 (Figure 7). In the second stage the gob stress distribution was analyzed during the.

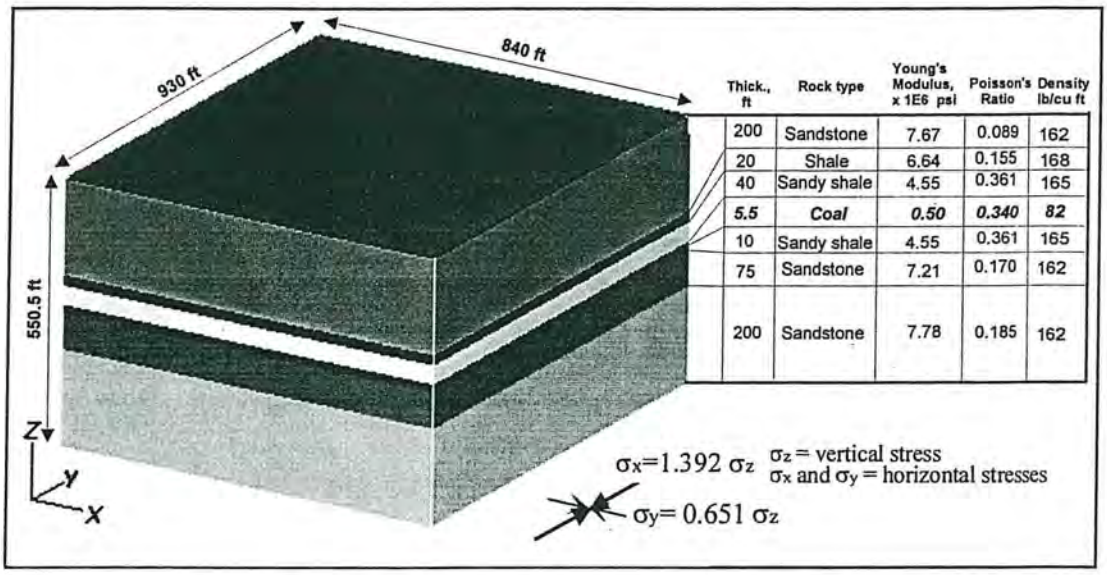

Thick., ft	Rock type	Young's Modulus, x 1E6 psi	Poisson's Ratio	Density lb/cu ft
200	Sandstone	7.67	0.089	162
20	Shale	6.64	0.155	168
40	Sandy shale	4.55	0.361	165
5.5	*Coal*	*0.50*	*0.340*	*82*
10	Sandy shale	4.55	0.361	165
75	Sandstone	7.21	0.170	162
200	Sandstone	7.78	0.185	162

Figure 6 3D model with mechanical properties of the rocks

retreat of panel S-9 and panel S-10. In the last stage, a comparison between the in-situ measurements and FE model results was conducted.

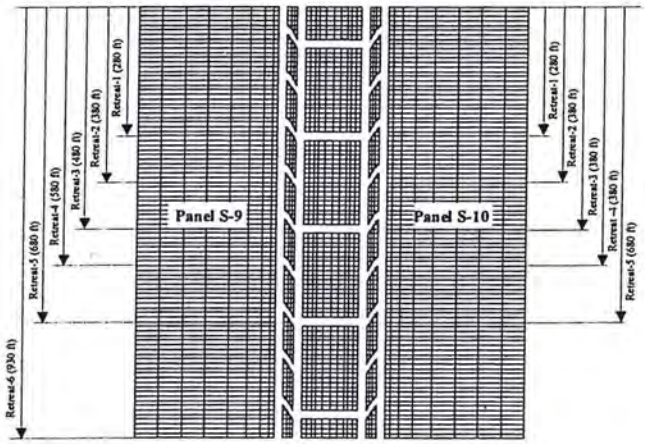

Figure 7 Retreat plan for longwall S-9 and S-10.

Figure 8 shows the stress-strain curve obtained by the ABAQUS simulation for a gob element at the center of panel S-9 at retreat No. 5. The simulated stress-strain curve shows a good agreement with the proposed gob model.

Figure 9 shows the distribution of the gob vertical stress along a longitudinal section x-x at the center of panel S-9 for retreat No. 5. It shows that the 85% of the virgin stress has been recovered at a distance of 400 ft from the face.

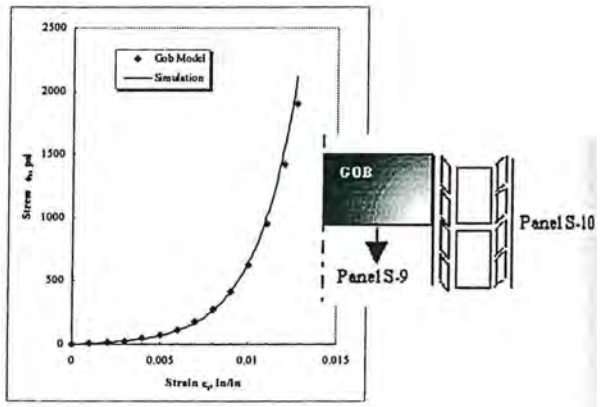

Figure 8 Comparison of simulated stress-strain curve and the proposed gob model

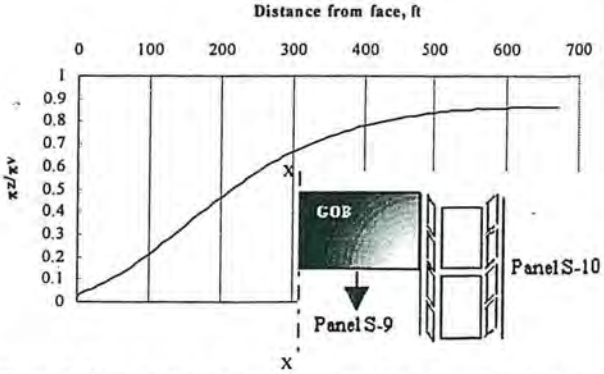

Figure 9 Distribution of vertical stress along x-x cross section.

Figure 10 shows the contour lines of vertical stress in the gob area of panel S-9 at different stages of longwall retreating. It shows a rapid increase in vertical stress from the start of the longwall mining until retreat step No. 3. Thereafter, the change in gob stress was small. Also, it shows the gob stress at the face and gateroad sides is approximately zero and builds up toward the center of the gob.

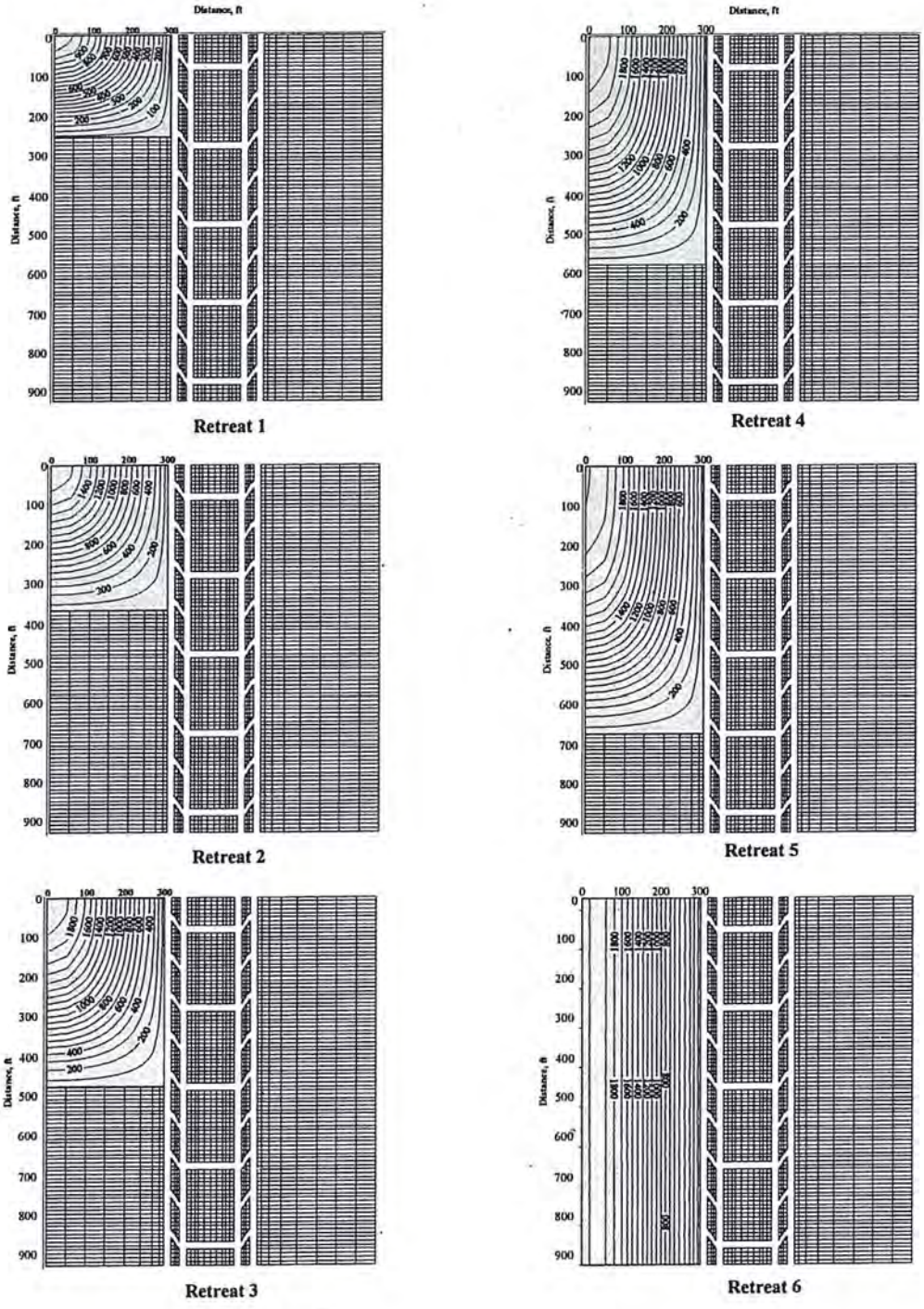

Figure 10 Vertical stress contours in gob area of panel S-9 at different stages of longwall retreat, (stresses are in psi).

Figure 11 shows the contour lines of vertical stress of panel S-10 at different stages of longwall retreating. The same gob behavior as that of panel S-9 was observed in panel S-10, i.e. it changed very little.

No significant change in the gob loading of panel S-9 observed during the mining of panel S-10. This could be due to elastic behavior which was assumed for the pillar system.

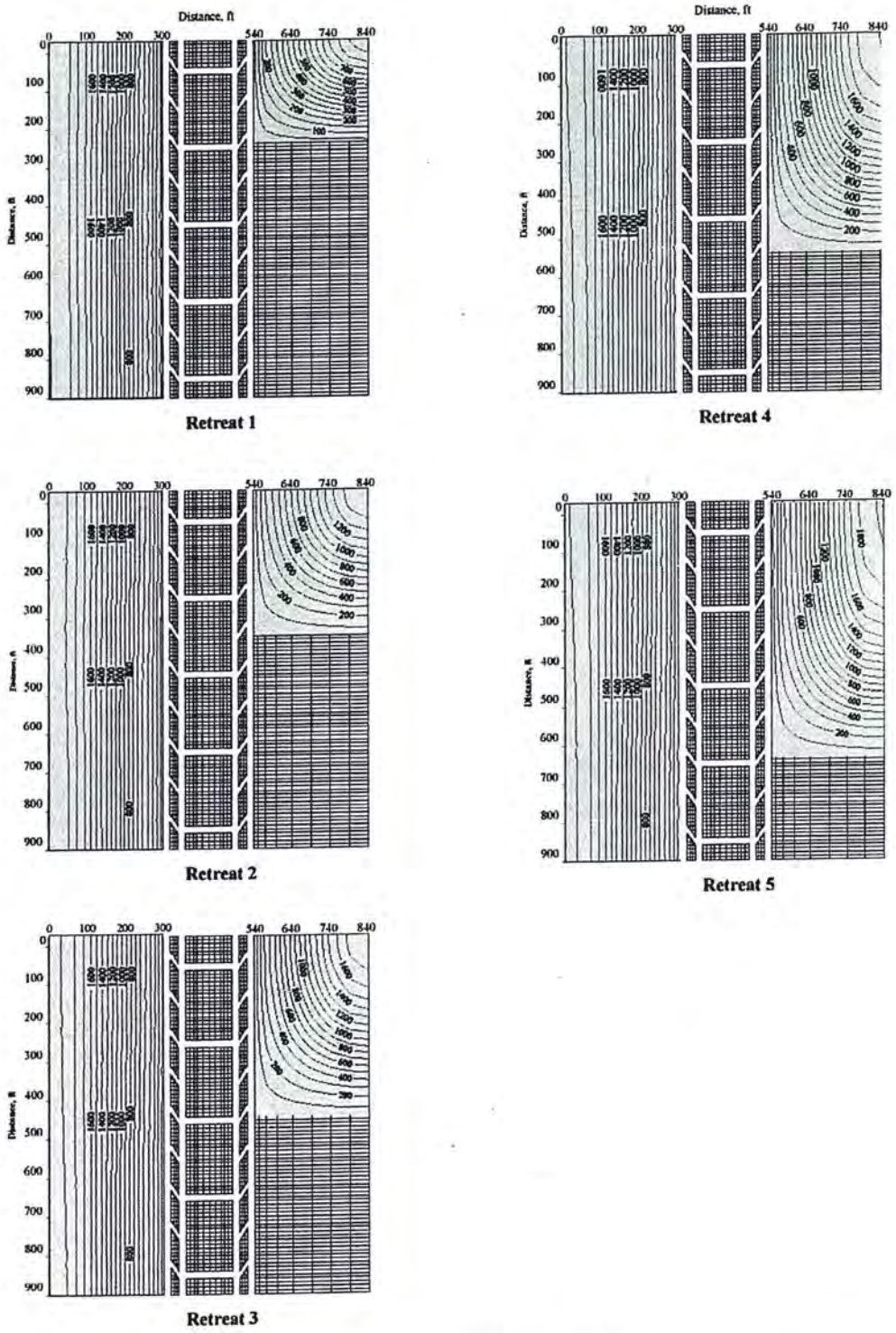

Figure 11 Vertical stress contours in gob area of panel S-10 at different stages of longwall retreat, (stresses are in psi)

In spite of the discrepancy existed in the monitored in-situ loading of longwall gob floor of panel S-9 and panel S-10, this was an excellent set of data for verification of the proposed gob model. Since the measured in-situ stresses were strongly affected by the orientation of BPF, the estimated values of the maximum and minimum principal stresses were used to show the upper and lower limits of the floor stress. Figure 12 shows a comparison between the measured and predicted floor stresses when the face of panel S-9 passes the monitoring stations. It shows a good agreement between the measured stresses and the estimated vertical stresses, except for three stations; 58 ft, 89 ft and 248 ft from the headgate. Except the station at 58 ft from the headgate, the vertical stresses at all other stations were within the limits of principal stresses..

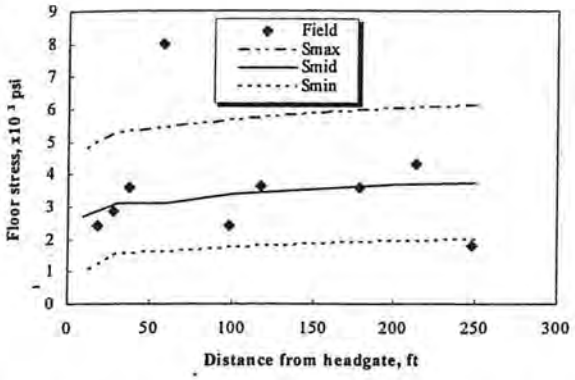

Figure 12 Vertical strees for floor under panel S-9 when the longwall face passes by the monitoring stations.

Figure 13 shows the peak stress recovery under panel S-9 that increases as the distance from the headgate increases. Figure 13 shows that the measured vertical stress recovery is within the limits of principal stresses. Figure 14 shows the floor stress at different longitudinal sections during the mining of panel S-9. It shows that the front abutment peak load did not occur at, but within 100 ft from, the face location. In Sections A and D, 28 ft and 248 ft from the headgate of panel S-9, respectively, the measured floor stresses were very close to the estimated minimum principal stresses. For Section B at 89 ft from the headgate of panel S-9, the measured floor stresses were in the range of the estimated vertical stresses and the minimum principal stresses. Finally, in Section C the measured floor stresses at a distance of 178 ft from the headgate were within the range of the estimated vertical stresses and the maximum principal stresses.

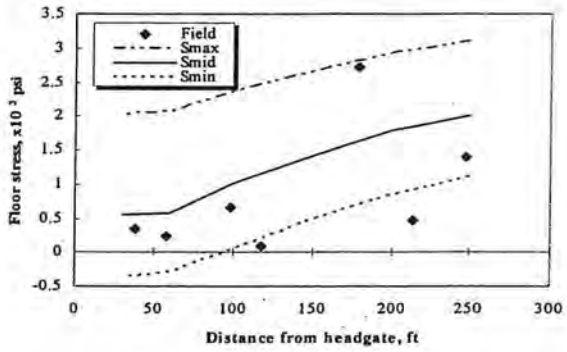

Figure 13 Peak stress recovery for floor under panel S-9 during panel S-mining

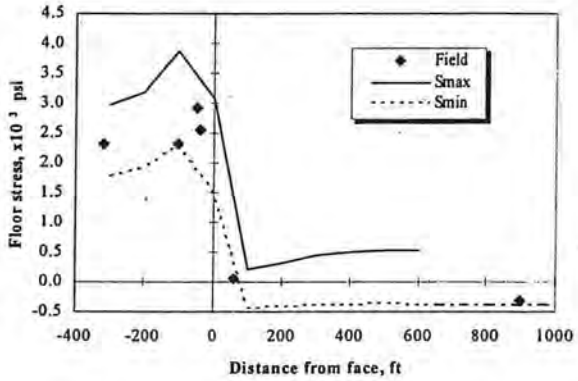

Section A (28 ft from the headgate of panel S-9)

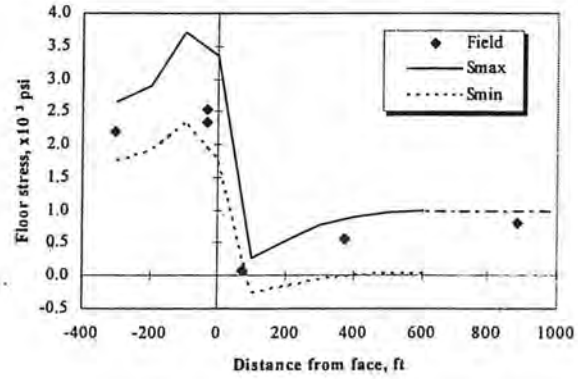

Section B (89 ft from the headgate of panel S-9)

Figure 14 Vertical stress for floor under panel S-9 at different monitoring stations during the retreat of panel S-9.

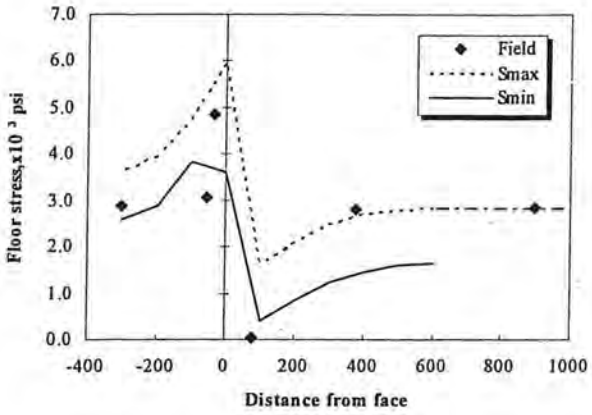

Section C (178 ft from the headgate of panel S-9)

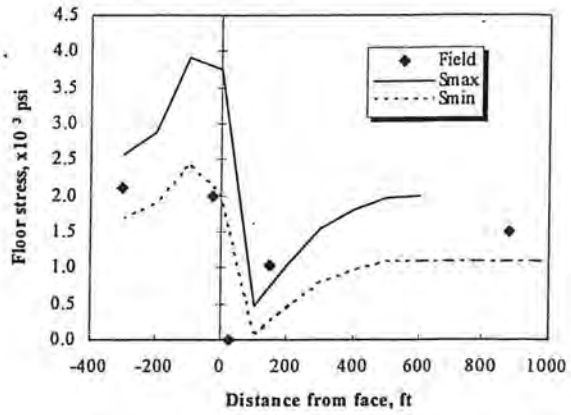

Section D (248 ft from the headgate of panel S-9)

Figure 14 cont.,

Unfortunately, the monitoring of floor stresses under panel S-10 was incomplete. Only a monitoring distance of 100 ft was recorded before the face reached the measurement stations and 30 ft of monitoring distance was recorded after the face passed the measurement stations. Figure 15 shows a comparison between the measured and predicted floor stresses when the face of panel S-10 passed the monitoring stations. It shows that the measured floor stress was close to the estimated vertical stresses, except for a station at a distance of 38 ft from the tailgate of panel S-10. This station showed a much higher stress than the estimated maximum principal stress.

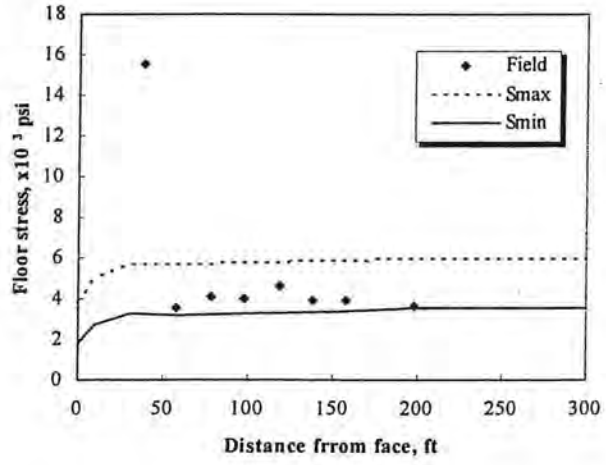

Figure 15 Vertical stress for floor under panel S-10 when the longwall face passes by the monitoring stations.

Conclusions

Unfortunately, most finite element packages do not have a ready-made model for gob material. However, these packages usually provide the user with an interface to define new material models. In this study, a gob model based on the Terzaghi's model was incorporated successfully into the comprehensive finite element package, ABAQUS, to simulate the loading behavior of longwall gob material.

The proposed technique does not require the division of the gob area into zones of different materials as it was used to be done before. Instead, one gob material is prescribed for the whole gob area and the stiffness of gob material is updated automatically during the solution according to the state of stress.

The proposed gob material shows the ability to transfer the abutment loads away from the face and chain pillar system towards the center of the gob area.

In spite the deviation of the model predictions from the in-situ measurements in some cases, it shows the same loading behavior.

Further work needs to be done to study the effects of some parameters such as the gob height factor (gob height–to-seam height ratio), the overburden depth, the model dimensions, etc. on the performance of the gob model.

Acknowledgement

This research was sponsored by CDC (NIOSH) through Grant No. G1R010H04238-01.

References

1. Karabin, G. J., and Evanto, M. A.," Experience with the Boundary-Element Method of Numerical Modeling to Resolve Complex Ground Control Problems," Proc. of the 2nd Int. Workshop on Coal Pillar Mech. and Design, NIOSH, IC 9448, 1999, pp. 89-113.
2. Hibbitt, D., Karlsoon, B., and Sorensen, P., "ABAQUS Manual," Version 5.8, Hibbitt, Karlsoon & Sorensen, Inc., 1998.
3. Unrug, K. and Szwilski, T., "Methods of Roof Cavability Prediction," Chapter 3 in State-of-the-Art of Ground Control in Longwall Mining and Mining Subsidence, SME, AIME, 1982, pp. 13.
4. Peng, S., Matsuki, K., and Su, W., "3-D Structural Analysis of Longwall Panels," Proc. 21st U.S. Symp. On Rock Mech., University of Missouri Rolla, 1980, pp. 44-56.
5. Whittaker, B. N. "An Appraisal of Strata Control Practice," Mining Engineer, Vol. 134, 1974, pp. 9-24.
6. Wilson, A. H. and Carr, F., "A New Approach to the Design of Multi-Entry Developments for Retreat Longwall Mining," Proc. of the 2nd International Conf. on Ground Control in Mining, Morgantown, WV, 1982, pp. 1-21.
7. Whittaker, B.N. and Singh, R.N., "Evaluation of the Design Requirements and Performance of Gate Roadways," The Mining Engineer, February 1979, pp. 541-556.
8. Trueman R., "A finite Element Analysis for the Establishment of Stress Development in Coal Mine Caved Waste," Mining Sci. and Tech., No. 10, 1990, pp. 247-252
9. Campoli, A. A., Barton, T. M., Dyke, F. C. V., and Gauna, M., 1993, "Gob and Gate Road Reaction to Longwall Mining in Bump-Prone Strata," RI 9445, U.S. Bureau of Mines.
10. Oyanguren, P. R., "Simultaneous Extraction of Two Potash Beds in Close Proximity," Chapter 32 in Proc. of the 5th Int. Strata Control conference, 1972, pp.5.
11. Pappas, D.M. and Mark, C., "Behavior of Simulated Longwall Gob Material," Bureau of Mines, RI 9458, 1993.
12. Ryder, J. A., and Wagner, H., "2D Analysis of Backfill as Means of Reducing Energy Release Rates at Depth," Chamber of Mines of South Africa, Research Organization, Research Report No. 47/78, 1978, pp. 22.
13. Salamon, M. D. G., "Mechanism of Caving in Longwall Coal Mining," Rock Mechanics Contributions and Challenges: Proc. of the 31st U.S. Sympos. of Rock Mechanics, Golden, Colorado, 1990, 161-168.

NOTICE
THIS MATERIAL MAY BE PROTECTED BY COPYRIGHT LAW (TITLE 17 U.S. CODE)

Proceedings
21st International Conference on Ground Control in Mining

Edited by

Syd S. Peng
Chairman and Charles T. Holland Professor
Department of Mining Engineering
College of Engineering and Mineral Resources
West Virginia University
Morgantown, WV, USA

Christopher Mark
Chief, Rock Mechanics Section
National Institute for Occupational Safety and Health (NIOSH)
Pittsburgh Research Laboratory
Pittsburgh, PA, USA

A. Wahab Khair and Keith Heasley
Professor and Associate Professor
Department of Mining Engineering
College of Engineering and Mineral Resources
West Virginia University
Morgantown, WV, USA

August 6-8, 2002
Lakeview Scanticon Resort & Conference Center, Morgantown, WV, USA

ISBN 0-939084-56-9

TN288
.I61